Self-assembly/condensation interplay in nano-to-microfibrillar silicified fibrin hydrogels

Kun Wang, Kevin Albert, Gervaise Mosser, Bernard Haye, Aline Percot, Céline Paris, Cécile Peccate, Lea Trichet, Thibaud Coradin

Self-assembly/condensation interplay in nano-to-microfibrillar silicified fibrin hydrogels

Kun Wang,[a] Kevin Albert,[a] Gervaise Mosser,[a] Bernard Haye,[a] Aline Percot,[b] Céline Paris,[b] Cécile Peccate,[c] Léa Trichet,[a] and Thibaud Coradin[*a]

[a] *Sorbonne Université, CNRS, Laboratoire de Chimie de la Matière Condensée de Paris, 75005 Paris, France.*

[b] *Sorbonne Université, CNRS, MONARIS, 75005 Paris, France.*

[c] *Sorbonne Université, Inserm UMRS974, Association Institut de Myologie, Centre de Recherche en Myologie, 75013 Paris, France.*

* Corresponding author: T.C

E-mail : thibaud.coradin@sorbonne-universite.fr

Tel : +33-144274018

Abstract

Fibrin-based gels are used in clinics as biological glues but their application as 3D cellularized scaffolds is hindered by processing and stability issues. Silicification of fibrin networks appears as a promising strategy not only to address these limitations but also to take advantage of the bioactivity of Si. However, it raises the question of the influence of silica sources on fibrin self-assembly. Here tetraethoxysilane, aminopropyltriethoxysilane and silica nanoparticles were used to design hybrid and nanocomposite fibrin-based hydrogels. By varying the concentration in silica source, we could evidence two regimes of interactions that depend on the extent of inorganic condensation. These interactions modulated the fibrillar structure of the fibrin network from more than 500 nm to less than 100 nm. These nanofibrillar hydrogels could exhibit higher mechanical properties than pure fibrin while preserving their capacity to support proliferation of myoblasts, opening promising perspectives for the use of fibrin-silica constructs in tissue engineering.

Keywords: Fibrin; Silica; Tissue engineering

1.Introduction

There is increasing evidence that, besides their structural role as particles, coatings, scaffolds and ceramics, silicon-based materials, including silicates, silica and bioglass, can have a biological effect on tissue regeneration [1-4]. On this basis, many biohybrid and bio-nanocomposite systems associating a biopolymer hydrogel with Si-containing phases have been described [6-13]. An important question is whether the presence of the mineral precursor – in hybrid materials [14] –, or particles – in composite approaches [15]-, may impact the biopolymer organization. Indeed, aqueous Si species are hydroxylated and, in most physiological situations, oligomeric and condensed phases bear a negative charge, making them prone to interact with a large set of biomolecules via hydrogen bonds and electrostatic interactions [16-19]. Another point to consider is the influence of the mineral phase on the cell-matrix interactions. As a matter of fact, there is an increasing body of evidence that extended domains of hydrated silica are not favorable to mammalian cells adhesion [20,21].

Based on its key role in the wound healing process, the fibrin protein is currently used in clinics as the main component of biological glue [22-24]. Because fibrin is, similarly to type I collagen [25-28], an excellent substrate for the adhesion, proliferation and differentiation of a wide variety of cells, it has also been widely used to design 3D host scaffolds for tissue engineering [29-35]. It therefore comes as a surprise that, while some studies have explored interactions between fibrinogen and silica surfaces and nanoparticles [36-39], fibrin has scarcely been considered as a biopolymer to form Si-containing hybrid or nanocomposite scaffolds [40]. This particular study evidenced that the interactions of fibrinogen, the precursor of fibrin, with several organosilanes at very low concentrations (< 0.1 mM) could promote or hinder myoblast proliferation.

In order to understand further silica-fibrin interactions, we have studied here the formation of silicified fibrin hydrogels with high silica amount, with the aim of understanding how condensed Si phases could modify fibrin self-assembly and how such modifications could impact the physical, structural and biological properties of the protein network. Tetraethoxysilane and aminopropyltriethoxysilane were chosen as precursors for hybrid materials while silica nanoparticles, whose diameter of *ca*. 150 nm was selected based on past investigations [15], were used to prepare nanocomposite hydrogels. Turbidity and rheological measurements were performed to evaluate the impact of the Si species on fibrillogenesis and fibrin gel formation on both the short and long term. These data could be correlated to structural variation in hydrogel nanostructure evidenced by electron microscopy. Insights about the protein-mineral interactions were gained from infra-red spectroscopy and circular dichroism studies. Finally, the ability of these silicified hydrogels to promote the proliferation of myoblasts was checked by viability tests. All these results were discussed taking into consideration the interplay between inorganic condensation and protein self-assembly and in the perspective of applying these new scaffolds to tissue engineering.

2. Experimental

2.1. Synthesis of fibrin-silica hydrogels

Fibrinogen (*fbg*) from bovine plasma was purchased from EMD Millipore. The pure fibrinogen solution at 6 $mg.mL^{-1}$ was prepared in a citrate buffer solution (pH 7.2). Fibrin gels were obtained by adding 0.5 µL of a 200 $U.mL^{-1}$ solution of thrombin (from bovine plasma) in phosphate buffer saline (PBS) to 1 mL of the fibrin solution. Pre-hydrolyzed solutions of tetraethoxysilane (*teos*) and aminopropyltriethoxysilane (*am*) were prepared at 10 mM and 100 mM by stirring overnight at room temperature in HCl 10^{-2} M (pH = 2). Silica nanoparticles (*np*) *ca*. 150 nm in diameter were obtained using the Stöber method and suspended in citrate buffer at a 100 mM silica concentration from the dried powder. Fibrinogen-silane initial solutions were prepared at pH 7.2 by mixing 150 µL of the fibrinogen stock solution (40 $mg.mL^{-1}$) with variable amounts of the 10 mM or 100 mM silane/silica nanoparticles solutions complemented with citrate buffer to a total 1 mL volume to achieve silane final concentrations of 1, 3, 5, 10 or 50 mM. Fibrin-silane gels were obtained by mixing the fibrinogen-silane solutions with 0.5 µL thrombin (200 $U.mL^{-1}$).

2.2. Kinetics study by turbidimetry

Fibrinogen or fibrinogen-silane/nanoparticles solutions (999.5 µL) were added into a 1.5 mL cuvette and the absorbance at λ = 400 nm was measured. After 30 s, the solution was transferred to an Eppendorf tube, 0.5 µL of thrombin solution was added and the mixture vortexed for 15 s before being transferred to a new cuvette, with a fixed duration of the whole process of 30 s. The time evolution of absorbance was then recorded for the next 29 minutes, at a rate of 15 measurements per minute.

2.3. Rheological studies

The evolution of the rheological properties of the gels was measured using a MCR 302 rheometer from Anton Paar. Fibrinogen or fibrinogen-silane/nanoparticles with added thrombin were placed on the sample holder fitted with cone and plate geometry with a fixed gap width. Measurements were performed at 37°C at constant amplitude and angular frequency ($\gamma = 0.1\%$, $\omega = 0.5$ rad.s^{-1}).

2.4. Scanning electron microscopy (SEM) analysis

Selected hydrogels were fixed with 4% paraformaldehyde for 1 h and then with 2.5% glutaraldehyde in cacodylate buffer for another hour at 4°C. Progressive dehydration was then performed using successive baths with increasing ethanol content. After drying in supercritical CO_2, samples were imaged using a Hitachi S-3400N microscope operating at 6-10 kV.

2.5. Transmission electron microscopy (TEM) analysis

Selected hydrogels were sequentially fixed with paraformaldehyde, glutaraldehyde and nuclear red. They were subsequently dehydrated using ethanol baths, progressively impregnated with propylene oxide and incorporated in araldite resin prior to sectioning (UC7 Leica microtome). 70 nm ultrathin sections were observed on a transmission electron microscope FEI Tecnai Spirit G2 operating at 120 kV. Images were recorded on a Gatan CCD Orius camera.

2.6. Fourier transform infrared (FTIR) spectroscopy

Hydrogels were put in the -80°C fridge overnight and then dried using vacuum freeze-drying (LABCONCO). FTIR spectra were recorded on a FTIR spectrometer ALPHA (Bruker,

Germany) in an Attenuated Total Reflectance (ATR) mode. Samples were directly placed the diamond crystal and pressed in order to have a good contact between the sample and the crystal. Every sample was subjected to 64 scans ranging from 4000 to 400 cm^{-1}.

2.7. Circular Dichroism (CD) measurements

Circular Dichroism (CD) spectra for the pure and *teos*-, *am*- and *np*-fibrinogen solutions without thrombin were recorded in the 185-300 nm range in Quartz cuvettes with an optical path length of 0.1 mm on a JASCO J810 spectropolarimeter. Mixed silane-fibrinogen solutions were prepared following the same protocol as for hydrogels preparation except that no thrombin was added. Mixed nanoparticles-fibrinogen solutions were prepared from 1 mL *fbg* (0.05 wt%) with different volumes of *np* solution (0.1 wt%) in *np*:*fbg* weight ratio varying from 0:1 to 2 :1. Each experiment was performed five times.

2.8. Myoblast cells encapsulation and 3D growth

C2C12 cells were grown in DMEM medium supplemented with 10% fetal bovine serum and 1% penicillin/streptomycin at 37°C in a humidified incubator with 5% CO_2, and passaged every 2 days. 1 mL of pure or silane/silica-fibrinogen solutions were mixed with 1mL of cell suspension at passage 14 containing 40,000 C2C12 cells, placed into wells of a 12-well plate, and then supplemented with thrombin to form gels. This procedure allowed to obtain hydrogels with final concentrations of fibrinogen and silanes/silica of 6 $mg.mL^{-1}$ and 10 mM, respectively. To check the effect of silanes/silica at a final concentration of 50 mM, if we used the same procedure, it would have been necessary to prepare initial silane/silica *np* solutions at 500 mM. However, such solutions were highly unstable upon neutralization.

Therefore an alternative protocol was developed for the preparation of 50 mM *am* and *np* gels, involving mixing 1 mL of 100 mM *np* or *am*, 300 µL of *fbg* (40 $mg.mL^{-1}$), 200 µL of citrate buffer and adding 500 µL of the cell suspension containing 40,000 C2C12 cells .

After the formation of gels, 1 mL of growth medium was added on the top of the gels. After 4, 6 and 8 days, the medium was discarded and 800 µL of the Alamar Blue reagent (0.1 $mg.mL^{-1}$ from ThermoFisher) was added to wells. After incubation at 37 °C for 4 h, the supernatant was collected and the fluorescence emission at 585 nm was used to calculate the percentage of reduction of Alamar Blue.

3. Results

3.1. Turbidimetry and rheological studies

The impact of tetraethoxysilane (*teos*), aminopropyltriethoxysilane (*am*) and 200 nm-silica nanoparticles (*np*) on the self-assembly of fibrin was first studied by turbidimetry, *i.e*. monitoring solution absorbance at 400 nm (OD_{400}), and rheology (storage modulus *G'* and loss modulus *G''*) (**Fig. 1** and **Fig. S1, Supplementary data**). These two methods are highly complementary as the former allows the monitoring of the fibrin gel setting on the short term (0-30 min) while the latter provides information on the further maturation of the network (0-24 h).

For the pure fibrinogen (*fbg*) solution, the initial absorbance was low (OD_{400} = 0.08) and remained stable for 1 min after thrombin addition. After this delay, turbidity increased rapidly and then much more slowly to reach a plateau at OD_{400} = 2.30 after 30 min. In the presence of 1 mM *teos*, the initial absorbance was not modified but the delay before rapid increase of turbidity was slightly longer and the final absorbance also slightly increased (OD_{400} = 2.36) (**Fig. 1(a)**). At 3 mM, the initial absorbance was higher and the initial delay was even more lengthened but final absorbance was similar to pure *fbg*. At 5 mM, initial

absorbance slightly increased further (OD_{400} = 0.11) but the initial delay was very significantly shorter and the final absorbance decreased. Finally, at 10 mM *teos*, the initial absorbance of the *fbg*/silane mixture was very high (OD_{400} > 2) and evolved to a very small extent after thrombin addition. Larger *teos* concentrations fully inhibited the gelation process. Such a non-monotonous variation of *fbg* self-assembly course with *teos* concentration was also observed on rheological measurements (**Table S1, Supplementary data**). For the pure protein/thrombin system, the storage modulus *G'* increased for *ca*. 7 h and reach a plateau at *ca*. 185 Pa. At 1 mM *teos*, the initial slope of *G'* increase was similar but both the time to reach plateau and the final *G'* were slightly higher (9 h, 210 Pa) (**Fig. 1(b)**).

At 3 mM, the initial slope was much smaller, the time required to reach stabilization was *ca*. 18 h and *G'* was *ca*. 150 Pa. At 5 mM *teos* had a similar effect to 3 mM but the stabilization time was further increased and the maximum *G'* value further decreased to *ca*. 120 Pa. A very different situation was observed for 10 mM for which an initial steeper increase of *G'* was measured for *ca*. 2h, followed by a second slower growth phase, the maximum *G'* value of *ca*. 175 Pa being reached after 10 h. Altogether, turbidimetry and rheology converge in showing that 1 mM *teos* concentration had a limited impact on fibrin self-assembly whereas 10 mM had a profound effect on the process. However, the clear impact of intermediate concentrations, and especially 3 mM, on the rheological properties of the gel could not be expected from their relatively minor influence on the turbidimetry curves, suggesting an evolution of *teos*/fibrin interactions with time.

The same remark applies in the presence of *am* but a higher concentration of this silane, compared to *teos*, seems necessary to observe a significant impact on *fbg* behavior (**Fig. 1(c,d)**). This is consistent with the fact that gels can be obtained at 50 mM with *am* whereas *teos* inhibited fibrin gel formation above 10 mM. From the turbidity curves, for concentrations from 1 mM to 10 mM, initial absorbance was not modified, initial delays were

slightly decreased and maximum absorbances were similar or slightly smaller than for pure *fbg*. At 50 mM, the delay was significantly smaller and the turbidity increase was much more abrupt, resulting in a clear increase in maximum OD_{400}. Meanwhile, maximum *G'* was slightly higher than pure *fbg* at 1 mM, decreased at 3 and 5 mM and then increased again at 10 and 50 mM, up to 325 Pa (compared to 185 Pa for pure *fbg*). The times required to reach maximum *G'* value also varies non-monotonously with increasing *am* content (**Table S1, Supplementary data**).

Considering silica nanoparticles, gels could also be obtained up to 50 mM *np* addition. The most striking evolution of turbidity curves was the progressive increase in initial absorbance with increasing *np* concentration. However, the final OD_{400} did not increase proportionally and the difference between maximal and initial absorbance decreased with increasing *np* concentration (**Fig. 1(e)**). In parallel, except for 1 mM *np*, there was a shortening of the initial delay and increase of the initial slope from 5 mM to 10 mM. The evolution at 50 mM was more complex to analyze, with a limited initial increase of OD_{400} followed by a slow evolution. When rheology measurements are considered, all *np*-containing hydrogels had higher maximum *G'* values than pure *fbg*, reaching more than 350 Pa at 50 mM (**Fig. 1(f)**). These composite gels also showed similar or longer times to reach *G'* plateau compared to the reference *fbg* hydrogel, with some minor variations with *np* content.

3.2. Electron microscopy studies

Hydrogel structure was examined by SEM after fixation and supercritical drying (**Fig. 2**). For pure *fbg* sample, a network of long fibers with diameters 150 ± 50 nm was observed (**Fig. 2(a)**). For *teos* at 5 mM, large fibers (> 250 nm) coexisted with much thinner ones (< 100 nm) (**Fig. 2(b)**). At 10 mM, these thin fibers coexisted with even larger fibrous structures that apparently consisted of fibers glued together by an amorphous material (**Fig. 2(c)**). With

am at 5 mM and 10 mM, fibers were thinner than *fbg* (100 ± 40 nm) (**Fig. 2(d,e)**). At 50 mM, a clear morphological change was evidenced with much larger fibrous structures (> 400 nm in diameter) that look unsheathed as for *teos* at 10 mM but, compare to this condition, the overall network appeared more homogeneous (*i.e*. absence of thin fibers) (**Fig. 2(f)**). In the case of *np*, at 5 mM, long fibers were observed, but again much thinner than for *fbg* (90 ± 20 nm) (**Fig. 2(g)**). Silica nanoparticles, either isolated or forming pearl necklace-like structures along the fibrin fibers, were also imaged. With increasing *np* concentration, no clear modification of the fibrous fibrin network could be evidenced but, at 50 mM, large aggregates of silica nanoparticles were observed (**Fig. 2(h,i)**).

Selected samples were also examined by TEM (**Fig. 3** and **Fig. S2, Supplementary data**). For the *fbg* sample, fibrin fibrils, *ca*. 150 nm in width were clearly visualized (**Fig. 3(a)**). In the presence of *teos* at 10 mM, fibrillar objects with various diameters, either larger or narrower than reference fibrin fibers, were imaged (**Fig. 3(b)**). While the presence of silica could be ascertained at lower magnification by the observation of a typical granular material (**Fig. S2, Supplementary data**), it was not possible to clearly distinguish a mineral phase at the vicinity of the fibrils at higher magnification. For *am* at 10 mM, the most striking observation was the presence of much thinner (< 100 nm) and often shorter fibrils (**Fig. 3(c)**). In contrast, fibrils significantly larger than in the *fbg* sample were observed in the presence of 50 mM *am* (**Fig. 3(d)**). However, it was again not possible to unambiguously identify the presence of a silica phase.

Finally, samples obtained with 10 mM *np* showed thin fibers either forming large aggregates with silica nanoparticles or dispersed in the surrounding medium (**Fig. S2, Supplementary data**). Increasing *np* concentration to 50 mM led to an increase in size of the nanoparticle/fibrin aggregates while some isolated even thinner fibrils could still be observed (**Fig. 3(e)**). Altogether, TEM confirmed the morphological evolution of the fibrils as a

function of silica source and concentration previously observed by SEM. However, except for nanoparticles, it was not possible to evidence any close fibrin-silica interface.

3.3. FTIR studies

To further investigate the fibrin-silica interface, the freeze-dried hydrogels were analyzed by ATR-FTIR spectroscopy. For fibrin alone, typical peaks of proteins were observed [41]. In the 3650-3000 cm^{-1} wavenumber range, a broad band including N-H stretching of Amide A/Amide B (*ca*. 3300 and 3100 cm^{-1}) and typical signatures of Amide I (1640 cm^{-1}), Amide II (1520 cm^{-1}) and Amide III (1240 cm^{-1}) were found [42,43]. The Amide I and II bands correspond to complex vibrations involving CO and NH and are very sensitive to protein conformation. It must be noticed that *teos* and silica have no reported vibration band in this wavenumber domain, so any change observed should sign for a modification of fibrin structure. As shown on **Fig. 4(a)**, an increase of the Amide I intensity (relative to Amide II) was observed as a function of added *teos* concentration. This can be attributed to a protein conformational change. In the presence of 1 and 5 mM *teos*, no major change could be evidenced except the presence of a new band near 3740 cm^{-1}, attributed to Si-OH [44]. For 10 mM *teos*, new bands appeared, a broad one between 1150 and 1000 cm^{-1}, attributed to the Si-O-Si, and a narrow one near 460 cm^{-1} corresponding to O-Si-O bending, both indicating *teos* condensation and silica formation. Changes were also expected for bands at 928 and 896 cm^{-1} (*i.e*. non-bridging Si-O and Si-O-Si bending) but no clear conclusion could be drawn as *fbg* also presents bands in this region.

A quite similar evolution was observed for *am* at 1 and 5 mM (**Fig. 4(b)**). In particular, it must be pointed out that the amine groups of *am* are expected to introduced some additional contribution near 1600 and 1500 cm^{-1} [45], preventing to attribute modifications in

the Amide I/amide II band ratio to conformational modification of fibrin only. Compared to *teos*, *am* introduced at 10 mM did not lead to a strong increase of absorbance in the 1150-1000 cm^{-1} region, suggesting that silane condensation remains limited at this concentration. In contrast, a very intense peak was obtained in this region for the 50 mM *am* content. In addition to the Amide band increase, important changes can be observed on the spectrum obtained at this concentration of *am*: increase of the bands at 3000, 1392, 1328, 1150-1000, 930 and 900 cm^{-1}. As previously mentioned, the band between 1150 and 1000 cm^{-1} can be attributed to the Si-O-Si stretching, whereas the band around 900 cm^{-1} can be associated to non-bridging Si-O groups. Noticeably, the concentrations at which significant silane condensation was ascertained by FTIR, *i.e.* 10 mM and 50 mM for *teos* and *am*, respectively, correspond to the conditions where turbidimetry and rheological measurements indicated a strong perturbation of fibrin self-assembly.

In the case of nanoparticles, the silica network is already condensed, as signed by the peaks at 1200-1000, 930 and 800 cm^{-1} (**Fig. 4(c)** and **Fig. S3, Supplementary data**). As observed for *teos*, as a function of *np* addition and from 5 mM, new bands appeared between 1150 and 1000 cm^{-1} and at 460 cm^{-1} evidencing the presence of silica, but no conformational change could be evidenced. For an addition of 50 mM *np*, a modification of the Amide I/Amide II relative intensity indicated a change in protein conformation.

3.4. Circular Dichroism studies

To check these hypotheses, the conformation of fibrinogen in the presence of silanes or nanoparticles was studied by Circular Dichroism (**Fig. 5**). For pure fibrinogen, the typical CD spectrum of this protein was obtained featuring one positive peak (I_1 @ λ_1 = 190 nm) and two negative signals (I_2 @ λ_2 = 209 nm and I_3 @ λ_3 = 220 nm) [46], with I_2 being more intense than I_3. No significant change in the relative intensity of the two negative signals was

observed in the presence of *teos* at 1 mM and 3 mM. However, at 5 mM, the decrease of I_2 intensity relative to I_3 was observed. This modification of intensity ratio was even more pronounced for *teos* at 10 mM. In the presence of *am*, a modification of the shape of the I_2 peak was observed for a silane concentration of 5 mM and 10 mM but the change in the relative intensity of I_2 and I_3 peaks appeared significant only at 50 mM. Taken together, these data support the existence of critical silane concentrations (10 mM for *teos* and 50 mM for *am*) where significant changes in fibrinogen concentration occur. In the case of nanoparticles, a progressive decrease of I_2 intensity relative to I_3 with increasing *np*:*fbg* ratio was observed and, for the highest investigated ratio, I_3 has become more intense than I_2. This confirms the above hypothesis that interactions of fibrinogen with silica nanoparticles can also modify its conformation.

3.5. Proliferation of C2C12 myoblasts

Proliferation of C2C12 myoblast cells within the hydrogels prepared at 10 mM *teos*, *am* or *np* was studied over 8 days by the Alamar blue test. As seen on **Fig. 6**, cells grew regularly in pure fibrin, *am*- and *np*-containing scaffolds. In the case of *teo*s, a low initial proliferation rate was observed over the first 6 days and then myoblast population increased much markedly but was still smaller than for pure fibrin.

Noticeably, attempts were made to grow C2C12 cells in the presence of 50 mM *am* and *np*. However, as described in the experimental section, the protocol required to achieve such a silica concentration in the hydrogels in the presence of cells imposed a lowering of the volume of added buffer solution. This apparently resulted in a much lower proliferation of cells in the fibrin-only reference (**Fig. S4, Supplementary data**). In these conditions, the presence of *am* and *np* had only a minor and short-term positive influence on proliferation over 8 days.

4. Discussion

The process of fibrin self-assembly as induced by thrombin addition is occurring in two steps [47-49]. In a first stage, thrombin cleaves one peptide located on the central E region of the protein. During this stage, only protofibrils are formed and the solution turbidity should remain stable and low. In a second stage, a second peptide is cleaved, leading to the full conversion of fibrinogen into fibrin, and the self-assembly process to form fibrils is triggered, resulting in an increase of turbidity [50-52]. The time between thrombin addition and beginning of turbidity increase is termed clotting or lag time and the slope of the turbidity curve indicates the kinetics of self-assembly [53]. A plateau is reached when all fibrin molecules are part of the hydrogel network. The final absorbance increases with the density and diameter of the fibrin fibrils, which depend on initial fibrinogen concentration and several other parameters such as pH or ionic strength [54-57]. Beyond the gel setting, maturation of the fibrin network occurs over several hours, leading to an evolution of the visco-elastic properties of the hydrogel as monitored by rheological measurements.

In the case of *teos*, up to 3 mM, neither the initial nor the final OD_{400} values were strongly modified compared to *fbg*, suggesting that little interactions existed between fibrinogen and hydrolyzed *teos* and that the structure of the fibrin network at the time of gel setting was similar to the pure *fbg* sample. However, on the longer term, *G'* value was significantly lower for 3 mM *teos* than *fbg*, suggesting a modification of the inter-fibrillar interactions. At 5 mM, turbidity increased as soon as thrombin was added and the final absorbance was slightly lower than the reference. This indicates significant interactions between fibrin molecules and hydrolyzed silane, impacting on the fibrin network structure. These interactions have a clear influence on the maturation of the hydrogel, with a much longer time required to reach the plateau and a final *G'* value nearly half that of pure *fbg*. At

this stage, FTIR and CD demonstrated a modification of the conformation of fibrin while SEM indicated a heterogeneous population of thin and large fibers. However, no condensation of *teos* could be evidenced. At 10 mM, mixing fibrinogen with pre-hydrolyzed *teos* led to an instant reaction, with a large increase of the initial optical density. Very importantly, thrombin addition did not lead to an important increase in absorbance but a hydrogel was formed, with ultimate *G'* value lower than pure *fbg* but higher than 5 mM *teo*s. In the meantime, *teos* condensation was evidenced by FTIR and silica nanoparticles were also observed together with fibrin fibers of various size in TEM and SEM images. Altogether, it seems that at such concentrations a hybrid fibrin-silica network was formed where both phases contributed to the structural and mechanical properties of the hydrogels. The fact that the self-assembly process of fibrin still occurred suggests that the conformational change indicated by FTIR and CD did not correspond to protein extensive denaturation but rather to its enhanced aggregation. This is supported by the observation of large fibers and is in agreement with a previous report showing that *teos* at low concentration (< 1 mM) can favor fibrinogen aggregation [40].

In the case of *am*, only minor modifications of the turbidity curves were observed up to 10 mM. At 50 mM, the initial OD_{400} was not increased but the lag time was much shorter, the slope was much larger and the plateau slightly higher than the reference. This would suggest that *am* does not interact strongly with fibrinogen but rather with fibrin and only at a significantly larger concentration than *teos*. This is supported by the CD measurements that show that, even at 50 mM, the conformational change of fibrinogen is less important than for *teos* at 10 mM. Noticeably, FTIR also allowed for correlating this concentration with the extended condensation of *am*, and also to an increase of the *G'* value, again pointing towards the formation of a hybrid hydrogels. However, whereas *teos* led to a heterogeneous distribution of fiber diameters, *am* leads to relatively homogeneous populations consisting of either nanofibrils (< 100 nm in diameter) at 10 mM or microfibrils (> 500 nm) at 50 mM.

Importantly, in the case of *np*, only nanofibrils were observed, either forming the protein network or within aggregates with silica nanoparticles. CD values clearly point out that fibrinogen and *np* were interacting without thrombin addition, but such interactions do not prevent fibrin gel formation. Moreover, the increase of *G'* with *np* content suggests that nanocomposites are formed. CD measurements also support the idea that fibrinogen and silica nanoparticles have significant interactions, which induce some conformational modification of the protein. However, CD data at low *np*:*fbg* ratios also indicate that excess (*i.e*. non-interacting) proteins preserve their initial structure.

Therefor two situations occur: compared to reference fibrin fibers *ca*. 150 ± 50 nm in diameter, either much narrower (<100 nm) nanofibrils or significantly larger (> 400 nm) microfibers were obtained. A decrease in diameter is usually associated with a decrease in fibrinogen concentration [57]. As a significant amount of fibrinogen can be adsorbed on the surface of *np*s, this should deplete the solution in available protein, thus explaining why the thinnest fibers were observed in the presence of silica nanoparticles. In parallel, an increase in fibrin fiber diameter would indicate favored aggregation of fibrinogen and/or fibrin [57,58]. In this context, a recent study showed that hydrophilic organosilanes such as *teos* and *am* can favor fibrinogen aggregation [40], which would explain why large fibers are obtained for the two silanes. It is however worth noting that 10 mM *teos* induced the simultaneous formation of both nano- and microfibrils while *am* led only to the former population at low concentration while the latter only formed at high concentration. This points out that organosilanes can play both roles, in a way that depends on their condensation extent but also on the nature of organic groups. In particular the ammonium function of *am* may not only modify the ionic strength of the medium but also interact with the protein *via* electrostatic interactions, both of which being able to influence fiber thickness [58]

The influence of such modifications on the mechanical properties of the hydrogels was also two-fold. In the case of *teos* and *am*, below what FTIR suggests to be a threshold concentration for condensation, *G'* values were lower than pure *fbg* and decreased with increasing silane amount whereas similar or even larger moduli were obtained above this threshold. This supports the hypothesis that the presence of silane interferes with the formation of the fibrin network but that the resulting loss of structural cohesion can be balanced by the formation of a continuous mineral network. In the case of *np*, it was noticed that despite the formation of narrower fibrils, *G'* values were always larger than pure *fbg*. This suggests that fibrin(ogen)/silica aggregates can act as reinforcing agents compensating the decrease of self-assembling proteins amount forming the proteinous fibrillar network.

From a biomaterial perspective, the presence of *am* or *np* at 10 mM allowed for C2C12 proliferation in a comparable extent to pure *fbg* whereas *teos* at the same concentration was detrimental to cell growth. The fact that the silicification process had no detrimental effect on cell behavior indicates that at these concentrations, neither the amino-silane nor the nanoparticles exhibit significant cytotoxicity towards the considered cells. Moreover, the modification of the structural features of the hydrogel, especially the formation of a nanofibrillar network, had no impact on cell adhesion. This is in agreement with recent results highlighting the benefits of nanofibrillar fibrin in tissue engineering [59,60]. In contrast the extended silica network formed by condensed *teos* does have a strongly negative impact on cell behavior within the hydrogels. This is in good agreement with previous reports devoted to collagen-based hybrid and nanocomposites suggesting that extended silica area present on protein surface are detrimental to cell adhesion and proliferation [20,21] whereas dispersed nanoparticles or amino-silane grafting may be more favorable [61,62]. It is also interesting to point out that while hydrogels containing 50 mM *am* and *np* could be easily prepared, their *in situ* cellularization could be achieved only by a modification of the

synthesis protocol due to the poor stability of the silane/silica precursor solution at neutral pH. This resulted in a marked decrease of cell proliferation inside the pure *fbg* prepared in similar conditions. Therefore, such silica-rich hydrogels are not adapted to 3D immobilization but may be of interest as scaffolds allowing cell infiltration and colonization.

Finally, it is important to emphasize that CD analyses have permitted to study the interactions between fibrinogen and silica sources whereas SEM, TEM, FTIR and rheological studies allowed for characterization of the fibrin-based hydrogels. However, once fibrinogen molecules have been converted to fibrin monomers by thrombin addition, these fibrin monomers stack as protofibrils which then assemble as fibrils [63]. Therefore, silica sources may also interact with these intermediate protofibrils. Another point to consider is the possible interaction of silanes and nanoparticles with thrombin. It has been reported that thrombin adsorption on porous silica nanoparticles could promote its clot forming ability by protecting it against anticoagulating factors. [64]. However, no specific study has examined the influence of organosilanes on thrombin, at least to our knowledge. Altogether, while interactions between silica sources and fibrinogen, and especially the clear difference between non-polymerized and polymerized silica, can explain some of our observations, other parameters would need to be investigated in more details to fully explain the here-reported morphological variations of fibrin fibers.

5. Conclusions

Fibrin-based hybrid and nanocomposite hydrogels were prepared over a large range of Si compositions that could show improved rheological properties while preserving the protein ability to support the proliferation and differentiation of muscle cells. It was possible to evidence an interplay between (organo)-silane condensation and fibrin self-assembly that

resulted in the modification of the nanostructure of the protein network. From a fundamental perspective, these results represent an original contribution to the understanding of the multi-faceted role that silicon species may play in physiological processes, especially in tissue formation and regeneration. More specifically, considering the key role of fibrinogen and fibrin in the coagulation cascade, it would be of great interest to look for a possible contribution of the natural or supplemented silicon content of blood on the clotting process. In parallel, these silicified scaffolds must now be evaluated *in vivo* for muscle tissue repair.

Conflicts of interest

There are no conflicts to declare.

Acknowledgments

KW thanks the China Scolarship Council for PhD funding and the Cluster of Excellence MATISSE (ANR-11-IDEX-0004-02) for additional financial support.

Appendix A. Supplementary data

Maximum *G'* and time to reach plateau; *G"* *vs*. time curves; additional TEM images; additional FTIR data; additional cell viability data

References

1. L.L. Hench, J.R. Jones, Bioactive glasses: frontiers and challenges, Front. Bioeng. Biotechnol. 3 (2015) 194.
2. Q. Yu, J. Chang, C. Wu, Silicate bioceramics: from soft tissue regeneration to tumor therapy, J. Mater. Chem. B 7 (2019) 5449-5460.
3. D.M. Reffitt, N. Ogston, R. Jugdaohsingh, H.F.J. Cheung, B.A.J. Evans, R.P.H. Thompson, J.J. Powell, G.N. Hampson, Orthosilicic acid stimulates collagen type 1 synthesis and osteoblastic differentiation in human osteoblast-like cells in vitro, Bone 32 (2003) 127-135.
4. S. Quignard, T. Coradin, J.J. Powell, R. Jugdaohsingh, Silica nanoparticles as sources of silicic acid favoring wound healing in vitro, Colloids Surf. B 155 (2017) 530-537.
5. X. Bourges, P. Weiss, G. Daculsi, G. Legeay, Synthesis and general properties of silated-hydroxypropyl methylcellulose in prospect of biomedical use, Adv. Colloid Interface Sci. 99 (2003) 215-228.
6. T. Coradin, J. Allouche, M. Boissière, J. Livage, Sol-gel biopolymer/silica nanocomposites in biotechnology, Curr. Nanosci. 2 (2006) 219-230.
7. A.R. Boccaccini, M.E. Erol, W.J. Stark, D. Mohn, Z. Hing, J.F. Mano, Polymer/bioactive glass nanocomposites for biomedical applications: a review, Compos. Sci. Technol. 10 (2010) 1764-1776.
8. O. Mahony, O. Tsigkou, C. Ionescu, C. Minelli, L. Ling, R. Hanly, M.E. Smith, M.M. Stevens, J. R. Jones, Silica ‐ gelatin hybrids with tailorable degradation and mechanical properties for tissue regeneration, Adv. Funct. Mater. 20 (2010) 3835-3845.
9. AJ. Mieszawska, N. Fourligas, I. Georgakoudi, N. M. Ouhib, D.J. Belton, C.C. Perry, D. L. Kaplan, Osteoinductive silk–silica composite biomaterials for bone regeneration, Biomaterials 31 (2010) 8902-8910.

10. S. Heinemann, T. Coradin, M.F. Desimone, Bio-inspired silica–collagen materials: applications and perspectives in the medical field, Biomater. Sci. 1 (2013) 688-702.
11. M.I. Alvarez Echazu, M.V. Tuttolomundo, M.L. Foglia, A.M. Mebert, G.S. Alvarez, M.F. Desimone, Advances in collagen, chitosan and silica biomaterials for oral tissue regeneration: from basics to clinical trials, J. Mater. Chem. B 4 (2016) 6913-6929.
12. S.-J. Wang, D. Jiang, Z.-Z. Zhang, Y. R. Chen, Z.-D. Yang, J.-Y. Zhang, J. Shi, X. Wang, J.-K. Yu, Biomimetic Nanosilica‐Collagen Scaffolds for In Situ Bone Regeneration: Toward a Cell‐Free, One‐Step Surgery, Adv. Mater. 31 (2019) 1904341.
13. K. Dashnyman, J. O. Buitrago, T. Bold, N. Mandakhbayar, R.A. Perez, J.C. Knowles, J.-H. Lee, H.-W. Kim, Angiogenesis-promoted bone repair with silicate-shelled hydrogel fiber scaffolds, Biomater. Sci. **7 (2019)** 5221-5231.
14. D. Eglin, K.L. Shafran, T. Coradin, C.C. Perry, Comparative study of the influence of several silica precursors on collagen self-assembly and of collagen on 'Si' speciation and condensation, J. Mater. Chem. 16 (2006) 4220-4230.
15. S. Bancelin, E. Derencière, V. Machairas, C. Albert, T. Coradin, M.-C. Schanne-Klein, C. Aimé, Fibrillogenesis from nanosurfaces: multiphoton imaging and stereological analysis of collagen 3D self-assembly dynamics, Soft Matter. 10 (2014) 6651-6657.
16. S.V. Patwardhan, G. Patwardhan, C.C. Perry, Interactions of biomolecules with inorganic materials: principles, applications and future prospects, J. Mater. Chem. 17 (2007) 2875-2884.
17. T. Coradin, J. Livage, Aqueous silicates in biological sol–gel applications: new perspectives for old precursors, Acc. Chem. Res. 40 (2007) 819-826.
18. H. Voisin, C. Aimé, T. Coradin, Understanding and tuning bioinorganic interfaces for the design of bionanocomposites, Eur. J. Inorg. Chem. 27 (2015) 4463-4490.

19. M. J. Limo, A. Sola-Rabada, E. Boix, V. Thota, Z.C. Westcott, V. Puddu, C.C. Perry, Interactions between metal oxides and biomolecules: from fundamental understanding to applications, Chem. Rev. 118 (2018) 11118-11193.
20. Y. Shi, C. Hélary, T. Coradin, Exploring the cell–protein–mineral interfaces: Interplay of silica (nano) rods@ collagen biocomposites with human dermal fibroblasts, Mater. Today Bio. 1 (2019) 100004.
21. Y. Shi, Y. Li, T. Coradin, Magnetically-oriented type I collagen-SiO_2@ Fe_3O_4 rods composite hydrogels tuning skin cell growth, Colloids Surf. B 185 (2020) 110597.
22. S. Kattuka, J.R. Byrnes, A.S. Wolberg, Fibrinogen and fibrin in hemostasis and thrombosis, Arterioscler. Thromb. Vasc. Biol. 37 (2017) e13-e21.
23. W.D. Spotnitz, Fibrin sealant: the only approved hemostat, sealant, and adhesive—a laboratory and clinical perspective, ISRN Surg. 2014 (2014) 203943.
24. PA. Janmey, J. P. Winer, J.W. Weisel, Fibrin gels and their clinical and bioengineering applications, J. R. Soc. Interface 6 (2009) 1-10.
25. R. Parenteau-Bareil, R. Gauvin, F. Berthod. Collagen-based biomaterials for tissue engineering, Materials 3 (2010) 1863-1887.
26. K. Lin, D. Zhang, M.H. Macedo, W. Cui, B. Sarmento, G. Shen, Advanced collagen-based biomaterials for regenerative biomedicine, Adv. Funct. Mater. 29 (2019) 1804943.
27. D. Gonipath, M.R. Ahmed, K. Gomathi, K. Chitra, P.K. Seghal, R. Jayakumar, Dermal wound healing processes with curcumin incorporated collagen films, Biomaterials 25 (2004) 1911-1917.
28. M. Xiao, L. Gao, A.R. Chandrasekaran, J. Zhao, Q. Tang, Z. Qu, F. Wang, L. Li, Y. Yang, X. Zhang, Y. Wan, H. Pei, Bio-functional G-molecular hydrogels for accelerated wound healing. Mater. Sci. Eng. C 105 (2019) 110067.

29. K.G. Cornwell, G.D. Pins, Discrete crosslinked fibrin microthread scaffolds for tissue regeneration, J. Biomed. Mater. Res. A 82 (2007) 104-112.

30. T.A.E. Ahmed, E.V. Dare, M. Hincke, Fibrin: a versatile scaffold for tissue engineering applications, Tissue Eng. Part B Rev. 14 (2008) 199-215.

31. A. Breen, T. O'Brien, A. Pandit, Fibrin as a delivery system for therapeutic drugs and biomolecules, Tissue Eng. Part B Rev. 15 (2009) 201-214.

32. F.M Shaikh, A. Callanan, E.G. Kavanagh, P.E. Burke, P.A. Grace, T.M. McGloughlin, Fibrin: a natural biodegradable scaffold in vascular tissue engineering, Cells Tissues Organs. 188 (2008) 333-346

33. A. Noori, S.J. Ashrafi, R. Vaez-Ghami, A. Hatamian-Zaremi, T.J. Webster, A review of fibrin and fibrin composites for bone tissue engineering, Int. J. Nanomed. 12 (2017) 4937-4961.

34. M.C. Barsotti, F. Felice, A. Balbarini, R. Di Stefano, Fibrin as a scaffold for cardiac tissue engineering, Biotechnol. Appl. Biochem. 58 (2011) 301-310.

35. R.L. Oage, C. Malcuit, L. Vilner, I. Vojtic, S. Shaw, E. Hedblom, J. Hu, G.D. Pins, M.W. Rolle, T. Dominko, Restoration of skeletal muscle defects with adult human cells delivered on fibrin microthreads, Tissue Eng. Part A 17 (2011) 2629-2640.

36. V. Gryshchuk, N. Galagan, Silica nanoparticles effects on blood coagulation proteins and platelets, Biochem. Res. Int. 2016 (2016) 2959414

37. A.A. Rugal, V.M. Gun'ko, V.N. Barvinchenko, V.V. Turov, T.V. Semeshkina, V.I. Zarko, Interaction of fibrinogen with nanosilica. Cent. Eur. J. Chem. 5 (2007) 32-54

38. A. Toscano, M.M Santore, Fibrinogen adsorption on three silica-based surfaces: conformation and kinetics, Langmuir 22 (2006) 2588-2597

39. K. Hyltegren, M. Hulander, M. Andersson, M. Skepö, Adsorption of fibrinogen on silica surfaces – the effect of attached nanoparticles, Biomolecules 10 (2020) 413

40. K. Wang, L. Trichet, C. Rieu, C. Peccate, G. Pembouong, L. Bouteiller, T. Coradin, Interactions of Organosilanes with Fibrinogen and Their Influence on Muscle Cell Proliferation in 3D Fibrin Hydrogels, Biomacromolecules 20 (2019) 3684-3695.

41. A. Barth, Infrared spectroscopy of proteins, BBA-Bioenergetics 1767 (2007) 1073-1101.

42. J.L.R. Arrondo, A. Muga, J. Castresana, F.M. Goni, Quantitative studies of the structure of proteins in solution by Fourier-Transform Infrared spectroscopy. Prog. Biophys. Molec. Biol 59 (1993) 23-56.

43. R.I. Litvinov, D.A. Faizullin, Y.F. Zuev, J.W. Weisel, The α-helix to β-sheet transition in stretched and compressed hydrated fibrin clots. Biophys. J. 103 (2012) 1020-1027.

44. F. Rubio, J. Rubio, J.L. Oteo, A FT-IR study of the hydrolysis of tetraethylorthosilicate (TEOS), Spectrosc. Lett. 31 (1998) 199-219.

45. R. Pena-Alonso, F. Rubio, J. Rubio, J.L. Oteo, Study of the hydrolysis and condensation of γ-Aminopropyltriethoxysilane by FT-IR spectroscopy, J. Mater. Sci. 42 (2007) 595-603.

46. Y. Chen, H. Mao, X. Zhang, Y. Gong, N. Zhao, Thermal conformational changes of bovine fibrinogen by differential scanning calorimetry and circular dichroism, Int. J. Biol. Macromol. 26 (1999) 129-134.

47. K. Laki, The polymerization of proteins: the action of thrombin on fibrinogen, J. Biol Chem. 222 (1951) 815-821.

48. J.D. Ferry, The mechanism of polymerization of fibrinogen, Proc. Natl Acad. Sci. USA 38 (1952) 566-569.

49. B. Blombäck, B. Hessel, D. Hogg, L.A. Therkildsen, A two-step fibrinogen–fibrin transition in blood coagulation, Nature 275 (1978) 501-505.

50. D.L. Higgins, S.D. Lewis, J.A. Shafer, Steady state kinetic parameters for the thrombin-catalyzed conversion of human fibrinogen to fibrin, J. Biol. Chem. 258 (1983) 9276-9282.

51. B. Blombäck, N. Bark, Fibrinopeptides and fibrin gel structure, Biophys. Chem. 112 (2004) 147-151.

52. H.A. Scheraga, The thrombin–fibrinogen interaction, Biophys. Chem. 112 (2004) 117-130.

53. B. Blombäck, M. Okada, Fibrin gel structure and clotting time, Thromb. Res. 25 (1982) 51-70.

54. A. Mathur, W.A. Schlapkohl, E. Di Cera, Thrombin-fibrinogen interaction: pH dependence and effects of the slow to fast transition, Biochemistry 32 (1993) 7568-7573.

55. B. Blombäck, K. Carlsson, K. Fatah, B. Hessel, R. Procyk, Fibrin in human plasma: gel architectures governed by rate and nature of fibrinogen activation, Thromb. Res. 75 (1994) 521-538.

56. N.A. Kurniawan, T.H.S. van Kempen, S. Sonneveld, T.T. Rosalina, B.E. Vos, K.A. Jansen, G.W.M. Peters, F.N. van de Vosse, G. H. Koenderink, Buffers strongly modulate fibrin self-assembly into fibrous networks, Langmuir 33 (2017) 6342-6352.

57. J.D. Ferry and P.R. Morrison, Preparation and properties of serum and plasma proteins. VIII. The conversion of human fibrinogen to fibrin under various conditions, J. Am. Chem. Soc. 69 (1947) 388-400.

58. S. Shulman. The effect of certain ions and neutral molecules on the conversion of fibrinogen to fibrin. Disc. Faraday Soc. 13 (1953) 109-115.

59. K. Stapelfeldt, S. Stamboroski, I. Walter, N. Suter, T. Kowalik, M. Michaelis, D. Brüggemann, Controlling the multiscale structure of nanofibrous fibrinogen scaffolds for wound healing, Nano Lett. 19 (2019) 6554-6563.

60. K. Stapelfeldt, S. Stamboroski, P. Mednikova, D. Brüggeman, Fabrication of 3D-nanofibrous fibrinogen scaffolds using salt-induced self-assembly, Biofabrication 11 (2019) 025010.

61. M. F. Desimone, C. Hélary, I.B. Rietveld, I. Bataille, G. Mosser, M.M. Giraud-Guille, J. Livage, T. Coradin, Silica–collagen bionanocomposites as three-dimensional scaffolds for fibroblast immobilization, Acta Biomater. 6 (2010) 3998-4004.

62. A. El-Fiqi, J.H. Lee, E.J. Lee, H. W. Kim, Collagen hydrogels incorporated with surface-aminated mesoporous nanobioactive glass: Improvement of physicochemical stability and mechanical properties is effective for hard tissue engineering, Acta Biomater. 9 (2013) 9

63. W.E. Fowler, R.R. Hantgan, J. Hermans, H.P. Erickson, Structure of the fibrin protofibril, Proc. Natl. Acad. Sci., USA 78 (1981) 4872-4876.

64. Y. Li, X. Liao, P. Liu, X. Shang, G. Ma, H. Chen, J. Fan, Surface group mediates the adsorption of in situ generated thrombin and its interaction with anti-thrombin in the protein corona of SBA-15, RSC Adv. 4 (2014) 21753-21756.

Captions

Fig. 1 Variation of absorbance at λ = 400 nm (a,c,e) and of storage modulus *G'* at 37° (b,d,f), as a function of time, of fibrinogen *fbg* solutions after thrombin addition in the presence of (a,b) *teos*, (c,d) *am* and (e,f) *np* at different concentrations (in mM). All experiments were made in triplicates and the curves show the resulting average data.

Fig. 2 SEM images of freeze-dried fibrin-based hydrogels. Scale bar: 2 μm

Fig. 3 Selected TEM images of freeze-dried fibrin-based hydrogels. Scale bar : 500 nm.

Fig. 4 (a-c) FTIR specta of freeze-dried hydrogels obtained from (a)*fbg*, (b)*fbg-teos*, (c) *fbg-am* and (d) *fbg-np* Spectra have been normalized to the Amide II band.

Fig. 5 Circular dichroism spectra of (a) *teos*-fibrinogen and (b) *am*-fibrinogen mixtures at various silane concentrations and (c) of silica nanoparticles-fibrinogen mixtures at various *np*:*fbg* weight ratios.

Fig. 6 Evolution of C2C12 proliferation within fibrin and fibrin-10 mM *teos*, fibrin-10 mM *np* and fibrin- 10 mM *am* hydrogels as monitored by Alamar Blue test. Error bars indicate standard deviation.

Fig.1

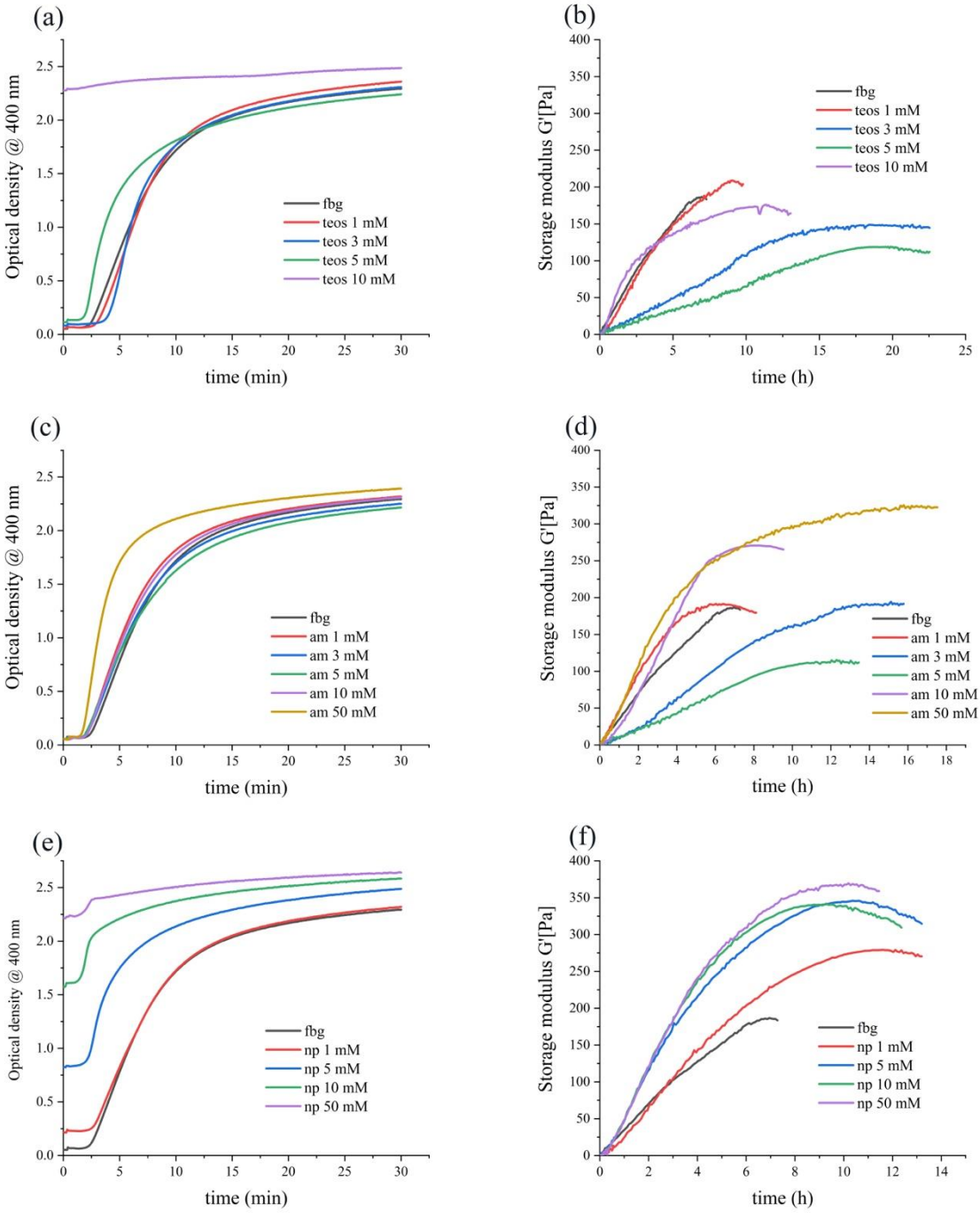
(a)
Optical density @ 400 nm
time (min)
fbg
teos 1 mM
teos 3 mM
teos 5 mM
teos 10 mM
(b)
Storage modulus G'[Pa]
time (h)
fbg
teos 1 mM
teos 3 mM
teos 5 mM
teos 10 mM
(c)
Optical density @ 400 nm
time (min)
fbg
am 1 mM
am 3 mM
am 5 mM
am 10 mM
am 50 mM
(d)
Storage modulus G'[Pa]
time (h)
fbg
am 1 mM
am 3 mM
am 5 mM
am 10 mM
am 50 mM
(e)
Optical density @ 400 nm
time (min)
fbg
np 1 mM
np 5 mM
np 10 mM
np 50 mM
(f)
Storage modulus G'[Pa]
time (h)
fbg
np 1 mM
np 5 mM
np 10 mM
np 50 mM

Fig.2

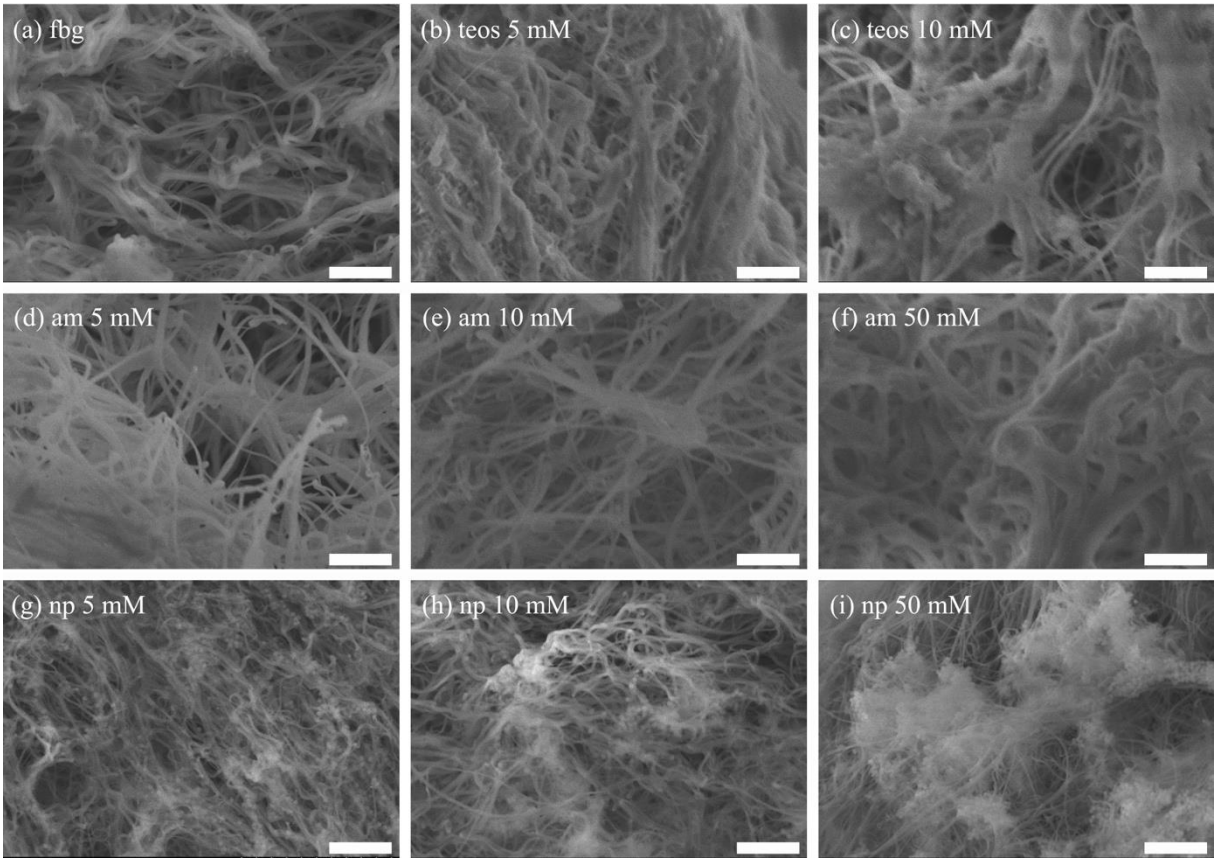
(a) fbg
(b) teos 5 mM
(c) teos 10 mM
(d) am 5 mM
(e) am 10 mM
(f) am 50 mM
(g) np 5 mM
(h) np 10 mM
(i) np 50 mM

Fig.3

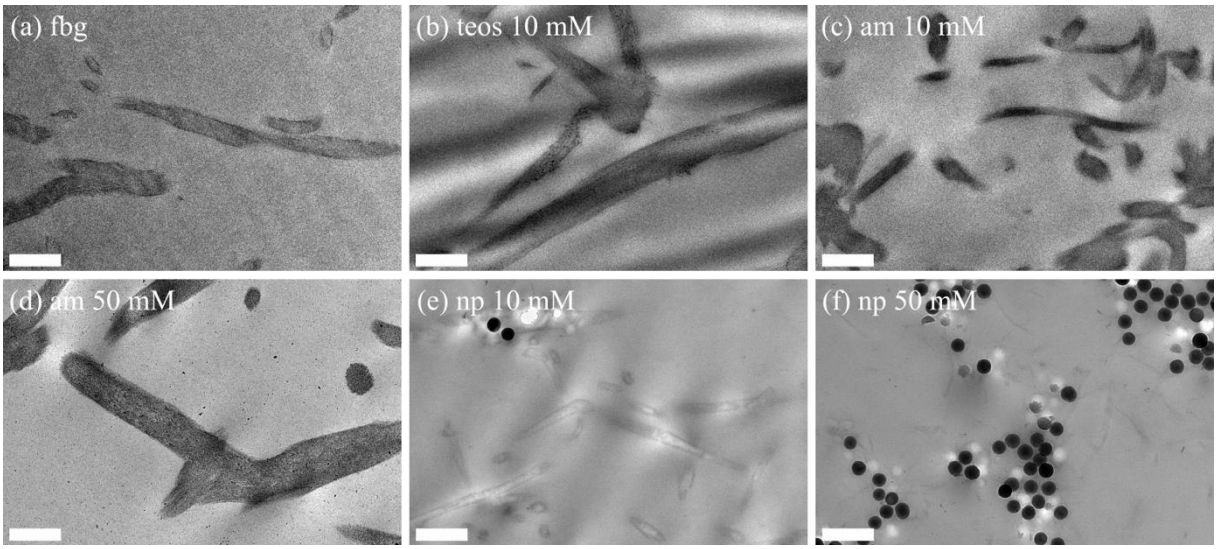

Fig.4

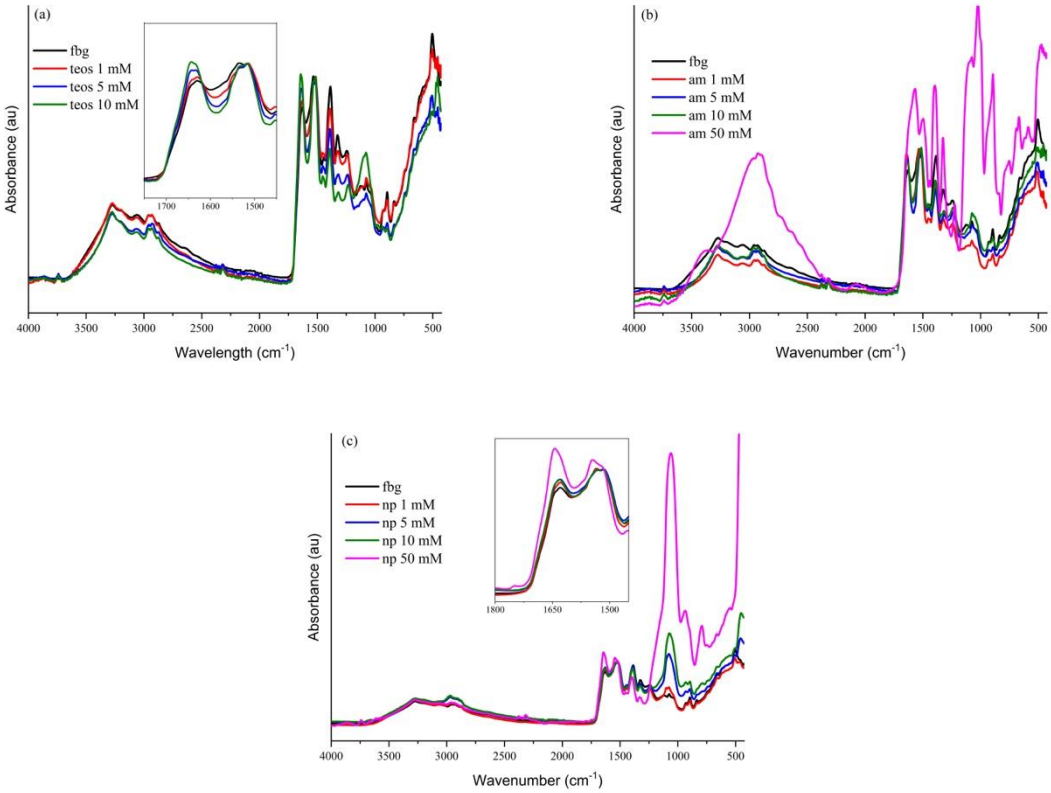
(a)
fbg
teos 1 mM
teos 5 mM
teos 10 mM
Absorbance (au)
Wavelength (cm-1)
(b)
fbg
am 1 mM
am 5 mM
am 10 mM
am 50 mM
Absorbance (au)
Wavenumber (cm-1)
(c)
fbg
np 1 mM
np 5 mM
np 10 mM
np 50 mM
Absorbance (au)
Wavenumber (cm-1)

Fig.5

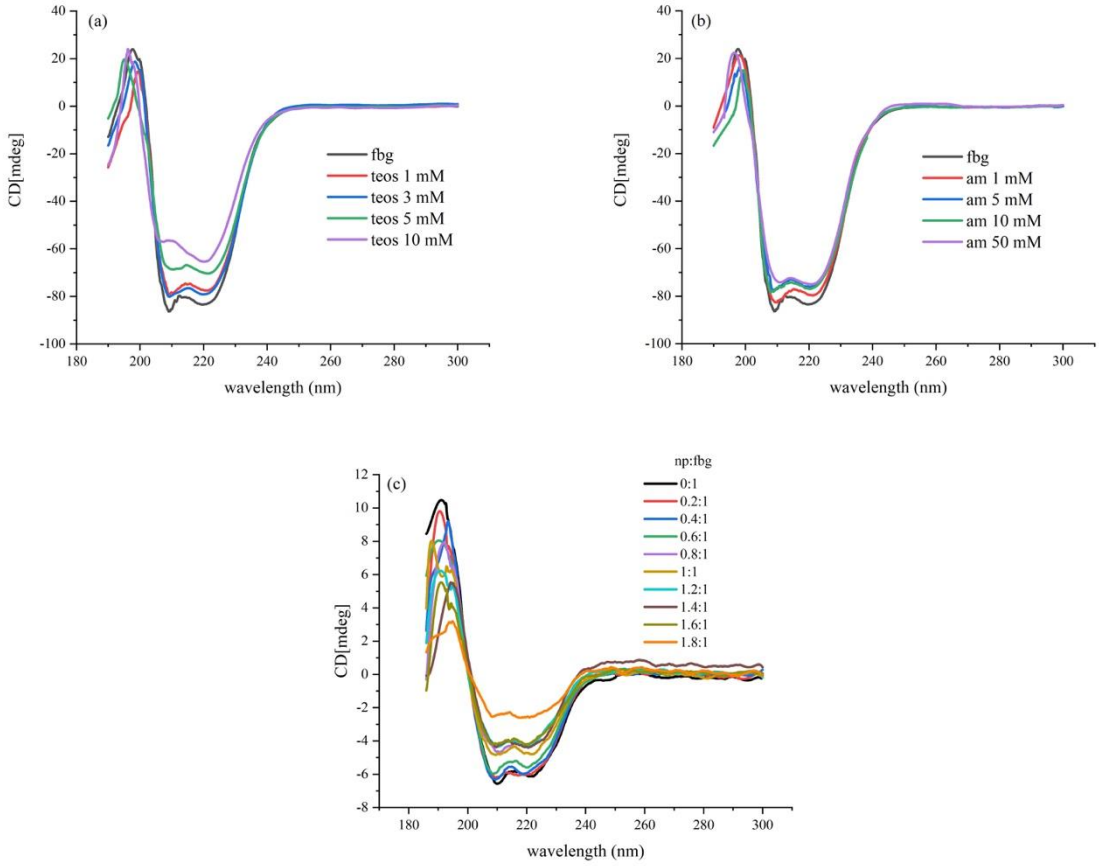
(a)
CD[mdeg]
wavelength (nm)
fbg
teos 1 mM
teos 3 mM
teos 5 mM
teos 10 mM
(b)
CD[mdeg]
wavelength (nm)
fbg
am 1 mM
am 5 mM
am 10 mM
am 50 mM
(c)
CD[mdeg]
wavelength (nm)
np:fbg
0:1
0.2:1
0.4:1
0.6:1
0.8:1
1:1
1.2:1
1.4:1
1.6:1
1.8:1

Fig.6

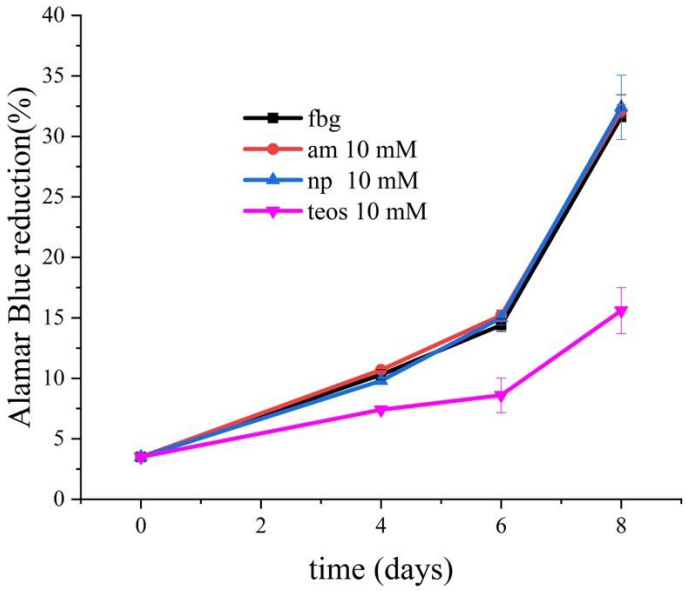
Alamar Blue reduction(%)
time (days)
fbg
am 10 mM
np 10 mM
teos 10 mM
0
5
10
15
20
25
30
35
40
0
2
4
6
8